CANCER

Cancer cells deploy lipocalin-2 to collect limiting iron in leptomeningeal metastasis

Yudan Chi[1], Jan Remsik[1], Vaidotas Kiseliovas[2], Camille Derderian[1], Ugur Sener[3], Majdi Alghader[1], Fadi Saadeh[1], Katie Nikishina[1], Tejus Bale[4], Christine Iacobuzio-Donahue[1,4], Tiffany Thomas[5], Dana Pe'er[2,6], Linas Mazutis[2,6], Adrienne Boire[1,3,7]*

The tumor microenvironment plays a critical regulatory role in cancer progression, especially in central nervous system metastases. Cancer cells within the cerebrospinal fluid (CSF)–filled leptomeninges face substantial microenvironmental challenges, including inflammation and sparse micronutrients. To investigate the mechanism by which cancer cells in these leptomeningeal metastases (LM) overcome these constraints, we subjected CSF from five patients with LM to single-cell RNA sequencing. We found that cancer cells, but not macrophages, within the CSF express the iron-binding protein lipocalin-2 (LCN2) and its receptor SCL22A17. These macrophages generate inflammatory cytokines that induce cancer cell LCN2 expression but do not generate LCN2 themselves. In mouse models of LM, cancer cell growth is supported by the LCN2/SLC22A17 system and is inhibited by iron chelation therapy. Thus, cancer cells appear to survive in the CSF by outcompeting macrophages for iron.

Spread of cancer cells into the cerebrospinal fluid (CSF)–filled leptomeninges is known as leptomeningeal metastasis (LM). This form of metastasis has become increasingly common (*1*) and is typically fatal within months (*2*). Under normal physiological conditions, the leptomeningeal space is isolated from the systemic circulation by the blood-CSF barrier. This anatomic compartment is hypoxic and contains sparse amounts of metabolic intermediates and micronutrients (*3*). In the setting of LM, the normally acellular CSF contains cancer cells as well as lymphocytes, macrophages, and neutrophils. Cancer cells within this microenvironment must therefore cope with oppressive metabolic constraints while evading immune responses. To elucidate the mechanisms by which cancer cells overcome these constraints, we first applied single-cell transcriptomic techniques to CSF collected from cancer patients harboring LM and then undertook functional studies in mouse models of LM.

Cancer cells within human spinal fluid express LCN2 and SLC22A17

Cancer cells in the CSF disseminate throughout the central nervous system. Within this compartment they are vastly outnumbered by immune cells, primarily macrophages and lymphocytes (Fig. 1A) (*4*). To explore cancer and immune cell responses to the nutritionally sparse CSF, we applied single-cell RNA sequencing (scRNA-seq) to cellular material collected from the CSF of five patients with LM (Fig. 1B and figs. S1 and S2). LM was secondary to breast cancer primaries in three patients and to non–small cell lung cancer primaries in two patients (table S1). After scRNA-seq, the proportions of each cell type within the CSF remained consistent with those identified by clinical analysis (fig. S3, A and B).

We found that all CSF cells showed upregulated expression of iron transport genes, consistent with functional iron deficiency within this anatomic space (fig. S3C). Hepcidin, a protein implicated in both inflammation and iron deficiency (*5*), was detected at higher concentrations in the CSF of cancer patients harboring LM relative to those without LM (fig. S3D). In contrast, CSF levels of the ubiquitous iron transporter transferrin were equivalent in the two groups of patients (fig. S3E). We found that whereas immune cells expressed canonical iron transporter transcripts, cancer cells expressed a diverse array of genes associated with iron binding and transport (fig. S3C). Of these, transcripts for a single iron-binding and receptor pair were expressed exclusively within the cancer cell population in all five patients: lipocalin-2 (LCN2) and solute carrier family 22 member 17 (SLC22A17) (Fig. 1, C and D). Protein expression corresponding to these single-cell transcriptional data was confirmed by enzyme-linked immunosorbent assay (ELISA) and flow cytometry of human CSF (fig. S3, F to H). Finally, in autopsy tissues, LCN2 and SLC22A17 protein expression was detected by immunofluorescence in the cancer cell population but not in the macrophage or monocyte populations (Fig. 1, E to H, and fig. S3, I to O).

LCN2, also known as neutrophil gelatinase-associated lipocalin (NGAL), is a β-barrel secreted protein that binds siderophore-complexed ferric iron with high affinity (*6*–*8*). SLC22A17 is a LCN2 transporter expressed in a various cell types, including cancer cells (*9*). To investigate the functional consequences of LCN2/SLC22A17 expression, we used three mouse models of LM generated through iterative in vivo selection (table S2). Unselected parental cells are nonspecifically metastatic; the LM subpopulation of cells (LeptoM) readily enter into and grow within the leptomeningeal space (*10*). The mouse lung adenocarcinoma (LLC-Par, LLC-LeptoM), human lung adenocarcinoma (PC9-Par, PC9-LeptoM), and human breast adenocarcinoma (MDA231-Par, MDA231-LeptoM) models all share key features of human LM (*11*).

Flow cytometry of CSF from the immunocompetent LLC-LeptoM mouse model revealed infiltrating cancer cells accompanied by lymphocytes, macrophages, and neutrophils (Fig. 2A). Concentrations of hepcidin and LCN2 were elevated in the CSF of mice with LM (fig. S4, A and B). LCN2 staining by immunohistochemistry was specific to cancer cells within the leptomeningeal space (fig. S4C). We also found higher levels of LCN2 mRNA and protein in LeptoM cells than in their parental (Par) counterparts (fig. S2, D and E). Although previous studies have documented LCN2 expression in activated macrophages within other anatomic sites (e.g., mammary fat pad) (*11*, *12*), we found that LCN2 was expressed by cancer cells and not macrophages within the leptomeningeal space (fig. S4F). LCN2 binds productively to three known receptors (SLC22A17, LRP2, and MC4R) (*13*, *14*). In both humans and mouse models, SLC22A17 constituted the major LCN2 receptor (Fig. 1, F and H, and fig. S4, G to J).

LCN2 promotes cancer cell growth within the leptomeningeal space in mice

We next investigated the functional relevance of LCN2/SLC22A17 in the CSF. We found that short hairpin RNA (shRNA)–mediated loss of LCN2 expression in LeptoM cells inhibited their growth within the leptomeninges in all three mouse models and conferred a survival benefit to the animals (Fig. 2, B and C, and fig. S5, A to G). In contrast, LCN2 knockdown did not alter the growth of LeptoM cells within iron-replete anatomic sites in vivo (fig. S5, H to J). Knockdown of the LCN2 receptor SLC22A17 phenocopied these results (Fig. 2, D and E, and fig. S5, K and L). Conversely, overexpression of LCN2 in parental cells with no propensity for growth in the leptomeninges promoted the growth of these cells in the leptomeningeal space and hastened the death of these animals (Fig. 2, F and G, and fig. S6). Together, these results support a mechanistic role for the LCN2/SLC22A17 axis in leptomeningeal cancer cell growth.

[1]Human Oncology and Pathogenesis Program, Memorial Sloan Kettering Cancer Center, New York, NY 10065, USA. [2]Computational and Systems Biology Program, Memorial Sloan Kettering Cancer Center, New York, NY 10065, USA. [3]Department of Neurology, Memorial Sloan Kettering Cancer Center, New York, NY 10065, USA. [4]Department of Pathology, Memorial Sloan Kettering Cancer Center, New York, NY 10065, USA. [5]Department of Pathology and Cell Biology, Columbia University College of Physicians and Surgeons, New York, NY 10032, USA. [6]Parker Institute for Cancer Immunotherapy, Memorial Sloan Kettering Cancer Center, New York, NY 10065, USA. [7]Brain Tumor Center, Memorial Sloan Kettering Cancer Center, New York, NY 10065, USA.
*Corresponding author. Email: boirea@mskcc.org

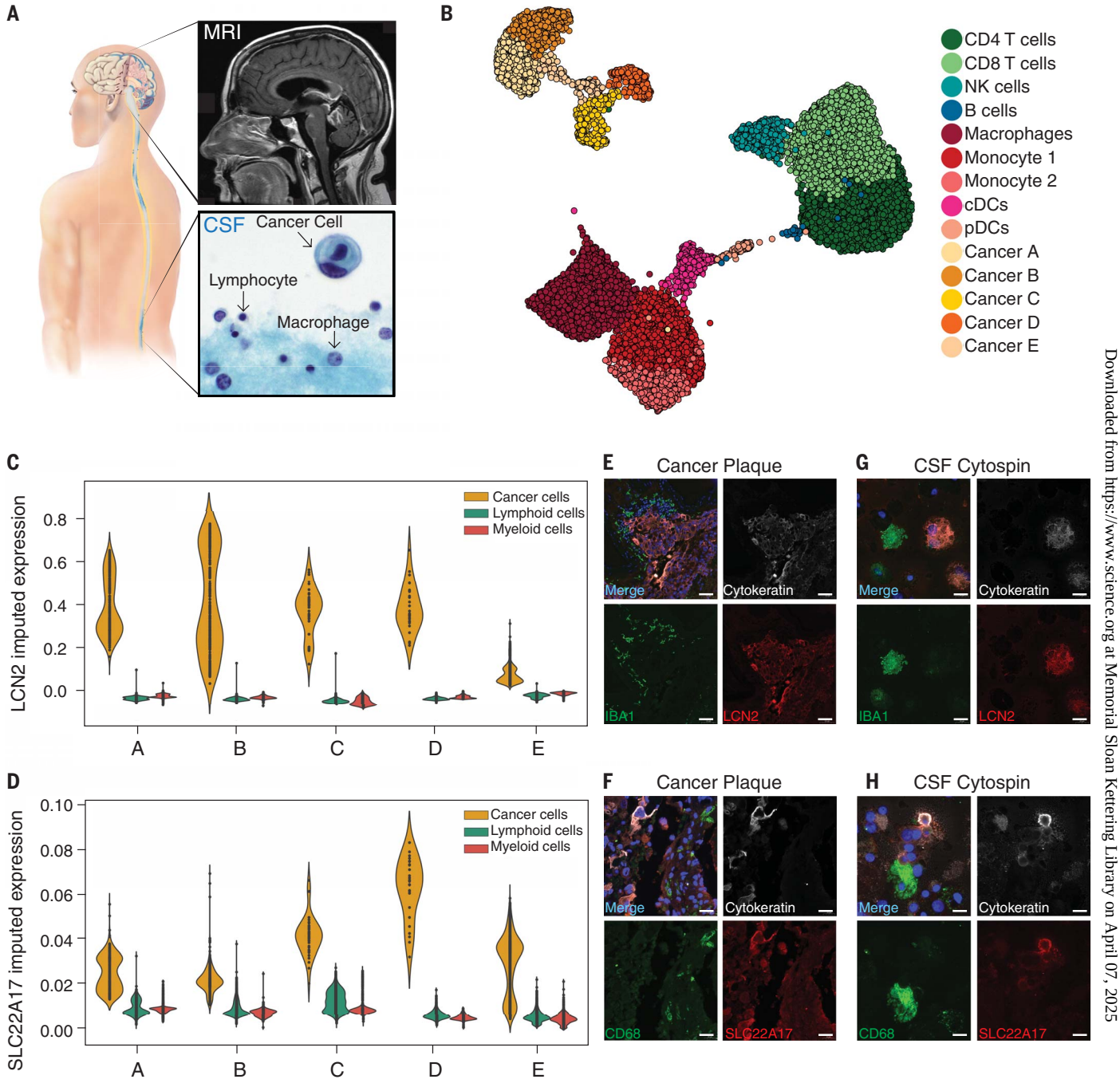

Fig. 1. Sparse CSF iron promotes LCN2 expression in cancer cells. (**A**) Human LM from breast cancer (patient B). White plaques of LM were visualized by magnetic resonance imaging (top right) and Giemsa-stained cytospin of CSF (bottom right). Major cell populations are indicated; the cytospin area pictured is 274 μm × 258 μm. (**B**) Single-cell transcriptional map of cancer and immune cells present in CSF of five patients, projected with uniform manifold approximation and projection (UMAP). Each dot represents a cell, colored by PhenoGraph cluster; major cell types are manually annotated according to fig. S1. Each individual patient is projected in fig. S2. (**C** and **D**) *LCN2* and *SLC22A17* gene expression in LM patients. Violin plots of *LCN2* (C) and *SLC22A17* (D) show imputed gene expression in cells from individual patients. All cells are grouped into three compartments: cancer cells (cancer patients A to E), lymphoid cells ($CD4^+$ T cells, $CD8^+$ T cells, B cells, NK cells), and myeloid cells [monocyte 1, monocyte 2, macrophage, conventional dendritic cells (cDCs), plasmacytoid dendritic cells (pDCs)]. (**E** and **F**) LCN2 (E) and SLC22A17 (F) detection by immunofluorescent staining of leptomeninges collected at autopsy from patients harboring LM. Cytokeratin (white) indicates cancer cells. Macrophages are indicated by the macrophage-specific proteins CD68 or ionized calcium-binding adaptor molecule 1 (IBA1) in green; LCN2 and SLC22A17 are shown in red. Images are representative of three cancer patients. Scale bars, 50 μm. (**G** and **H**) LCN2 (G) and SLC22A17 (H) expression assessed by cytospin staining of cancer cells and macrophages in CSF collected post mortem from patients in (E) and (F). Scale bars, 20 μm.

Inflammatory cytokines induce LCN2 expression in cancer cells

We next explored the mechanism leading to LCN2 expression in cancer cells within the LM. Downstream of both STAT and NF-κB transcriptional promoters, expression of LCN2 may be induced by a variety of inflammatory stimuli (*15*, *16*). To assess the inflammatory state of cells during LM, we queried the scRNA-seq dataset and found high expression levels of transcripts downstream of JAK-STAT and NF-κB promoters in the macrophage population (Fig. 3A and fig. S7A). Consistent with this, inflammatory cytokine (IL-6, IL-8, and IL-1β) concentrations were significantly higher in the CSF of cancer patients with LM than in control patients without LM (fig. S7B). This was also observed in mouse models (fig. S7, C and D). We hypothesized that macrophage-generated cytokines stimulate cancer cell LCN2 expression in the CSF.

To test this hypothesis, we cocultured LeptoM cancer cells with supernatant collected from macrophages freshly isolated from either the CSF or spleen of mice harboring LLC-LeptoM or LLC-Par tumor cells (Fig. 3B and fig. S7E). We found that macrophages from the CSF of mice harboring LM strongly induced LCN2 expression in LeptoM cancer cells (Fig. 3C). Coculture of these CSF macrophages with LeptoM cancer cells induced expression of LCN2 in cancer cells but not in macrophages (Fig. 3D). Outside the leptomeninges, LCN2 expression by macrophages/monocytes and neutrophils is typically induced by inflammation (*17*). In our models, although LCN2 expression was increased in extracranial splenic monocytes and neutrophils after lipopolysaccharide (LPS) treatment, LCN2 expression remained unchanged in these cells in the

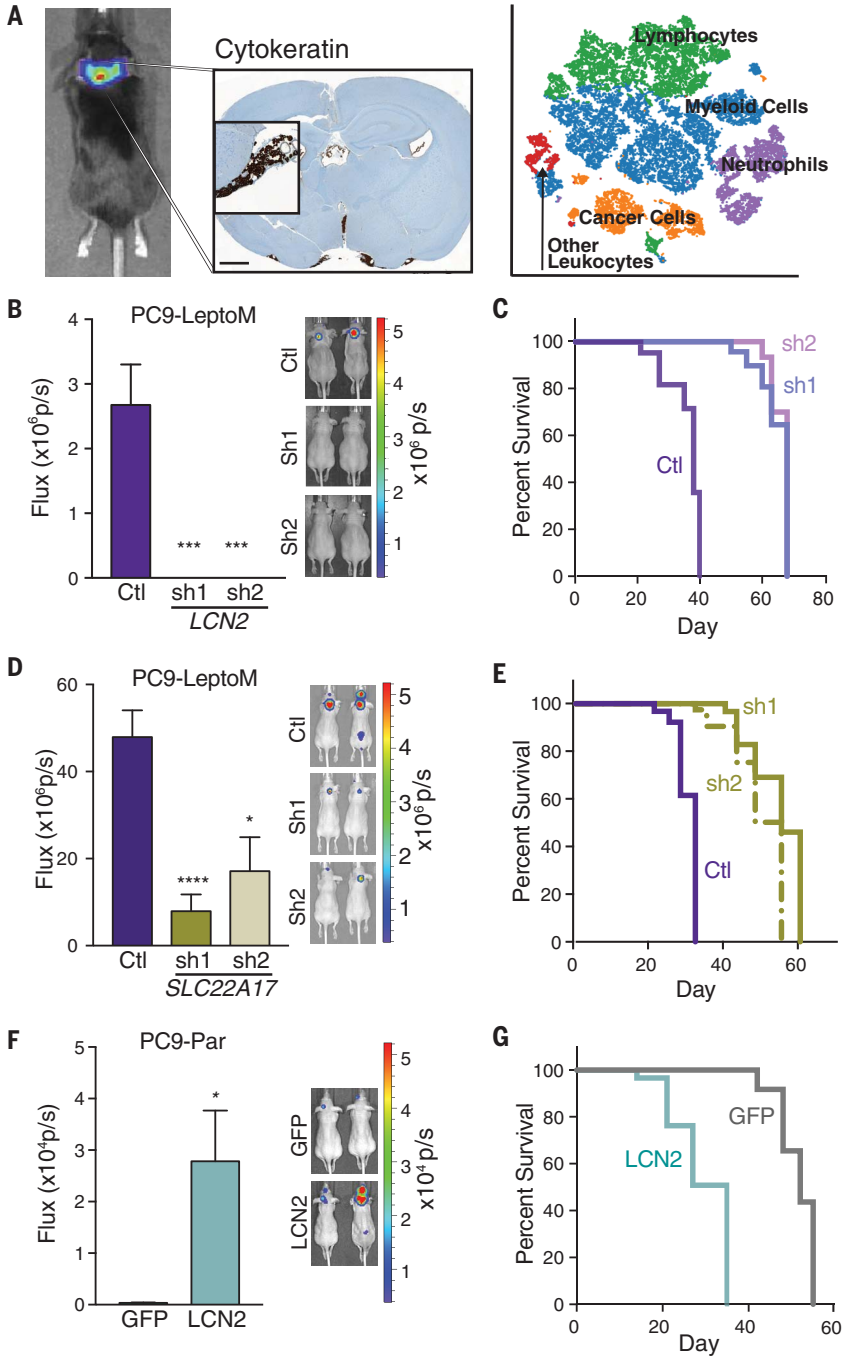

Fig. 2. LCN2 supports cancer cell growth in the leptomeninges. (**A**) Mouse model of LM. Left: In vivo bioluminescence imaging (BLI) of the LLC model at day 14 after intracardiac dissemination. Center: Immunohistochemistry for pan-cytokeratin. Scale bar, 1000 μm for larger image, 50 μm for inset. Right: t-distributed stochastic neighbor embedding (tSNE) of multicolor flow cytometry of CSF collected from syngeneic LLC mouse model (day 14). Major cell types: orange, cancer cells ($CD45^-$); purple, neutrophils ($CD45^+CD11b^+Ly6G^+$); green, lymphocytes ($CD45^+CD3^+$); blue, myeloid cells ($CD45^+CD11b^+$ excluding neutrophils); red, other leukocytes ($CD45^+CD11b^-Ly6G^-CD3^-$). A representative sample is shown; n = 5 mice. (**B**) Tumor growth in mice injected with PC9-LeptoM cells expressing either shCtl or shLCN2. Two independent shRNAs (sh1 and sh2) were used to target human *LCN2*. Left: Histogram represents in vivo BLI imaging after inoculation at day 28; n = 8 to 10 per group in each of two independent experiments. Right: Representative BLI images. ***$P < 0.001$ (unpaired t test). Data represent mean ± SEM. (**C**) Kaplan-Meier survival curve of mice shown in (B). $P < 0.0001$. (**D**) Tumor growth in mice injected with PC9-LeptoM cells expressing either shCtl or shSLC22A17. We used two independent shRNAs (sh1 and sh2) to target human *SLC22A17*. Left: Histogram represents in vivo BLI imaging at day 28 after inoculation. n = 8 to 10 per group in each of two independent experiments. Right: Representative BLI images. *$P < 0.05$, ****$P < 0.0001$ (unpaired t test). Data are means ± SEM. (**E**) Kaplan-Meier survival curve of mice shown in (D). $P < 0.0001$. (**F**) Tumor growth in mice injected with PC9-Par cells expressing either green fluorescent protein (GFP) or LCN2. Left: Histogram represents in vivo BLI imaging after inoculation at day 21. n = 8 to 10 per group in each of two independent experiments. Right: Representative BLI images. *$P < 0.05$ (unpaired t test). Data represent mean ± SEM. (**G**) Kaplan-Meier survival curve of mice shown in (F). $P < 0.0001$.

CSF (figs. S3G, S4F, and S7F). Moreover, although LCN2 may induce influx of neutrophils to extracranial sites (*18*), we did not observe LCN2-dependent changes in CSF leukocyte composition (fig. S7G).

To identify the relevant cytokines in human disease, we immune-depleted select inflammatory cytokines from LM-positive human CSF (Fig. 3E). Whereas whole CSF from LM patients strongly induced LCN2 expression in cancer cells, immune depletion of IL-6 and/or IL-8 or inhibited this biological effect in both PC9 and MDA231 model systems (Fig. 3F and fig. S8A). Conversely, addition of recombinant IL-6, IL-8, and/or IL-1β to artificial CSF induced expression of LCN2 from PC9, MDA231, or LLC (fig. S8, B to D) LeptoM cells. Together, these data indicate that macrophage-generated cytokines induce expression of LCN2 in cancer cells within the LM.

To gain more insight into the properties of these proinflammatory leptomeningeal macrophages, we examined the transcriptome of the macrophage/monocyte population in our scRNA-seq dataset. Consistent with the known transcriptional heterogeneity of these cells (*19*), we observed nonreciprocal expression of both M1 (proinflammatory) and M2 (anti-inflammatory) polarization transcriptional gradients (fig. S8E). Unexpectedly, this analysis revealed the hypoxia transcriptional signature as a major feature of this macrophage population.

LCN2 supports cancer cell growth in the hypoxic leptomeninges in mice

Hypoxia signaling is intimately linked to iron homeostasis (*20*). We found that freshly isolated CSF cancer cells and immune cells from human LM samples showed evidence of hypoxia-induced transcriptional changes as well as a correlation between hypoxia and iron metabolic signatures (Fig. 4, A and B, and fig. S9A). In mouse models, bulk RNA-seq of LeptoM derivative cell lines with and without LCN2 knockdown revealed LCN2-dependent expression of the hypoxia transcriptional signature, suggesting a role for LCN2 in hypoxia (Fig. 4C and fig. S9, B and C).

The biological relevance of hypoxia signaling in LM remains undetermined. In the absence of disease, the CSF is hypoxic, with partial pressure of O_2 ranging from 65 to 130 ± 49 mmHg. However, in inflammatory injury (*21*) or an impaired blood-CSF barrier (*11*), CSF oxygenation is improved. To study hypoxia in our LM mouse models, we generated a dual-luciferase reporter system consisting of constitutive firefly luciferase and nano-luciferase downstream of hypoxia response elements. The PC9-LeptoM and LLC-LeptoM models demonstrated NLuc activation (an indication of hypoxia) upon inoculation into the CSF, and this activation remained stable over the disease course (Fig. 4D). Despite this hypoxia, the

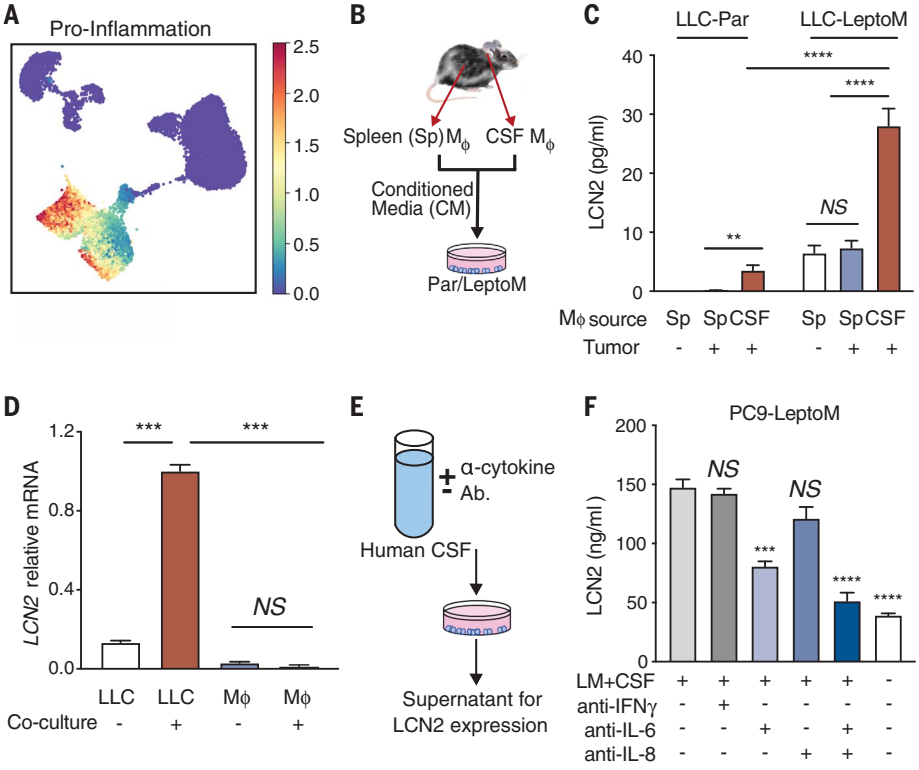

Fig. 3. Cancer cells generate LCN2 in response to inflammatory cytokines. (**A**) Mean expression of canonical proinflammatory cytokines from single-cell transcriptomics. Markov affinity-based graph imputation of cells (MAGIC)–imputed cytokine expression was standardized to zero mean and unit of standard deviation. See the proinflammatory cytokine dataset in table S5. (**B**) Schematic for cancer cell coculture with supernatant from macrophages in LLC-LeptoM model. Conditioned media was collected from macrophages, freshly sorted from CSF or spleen of C57Bl/6 mice harboring LLC-LeptoM cells or no cancer by fluorescence-activated cell sorting (FACS), and added to cultures of Par cells or LeptoM cells for 14 days, exchanging fresh conditioned media every 3 days. (**C**) Evaluation of LCN2 levels by ELISA in conditioned media generated as in (B); $n = 3$ in each of two independent experiments. $^{**}P < 0.01$, $^{****}P < 0.0001$ (unpaired t test); NS, not significant. Data are means ± SEM. (**D**) *LCN2* mRNA detection by quantitative polymerase chain reaction in CSF-derived macrophages and LLC-LeptoM cells after coculture at day 14; $n = 3$ in each of two independent experiments. $^{***}P < 0.001$ (unpaired t test). Data are means ± SEM. RLU, relative luminescence unit. (**E** and **F**) CSF from patients harboring LM was treated with neutralizing antibodies to IL-6, IL-8, or IFN-γ and added to PC9-LeptoM cells for 12 hours. LCN2 was quantified by ELISA in conditioned media 24 hours after removing CSF; $n = 3$ in each of two independent experiments. $^{***}P < 0.001$, $^{****}P < 0.0001$ (unpaired t test). Data are means ± SEM.

LeptoM cells continued to grow and expressed hypoxia-inducible factors HIF-1α and HIF-2α (Fig. 4, D and E, and fig. S9, D and E). In vitro, LeptoM derivatives demonstrated robust growth under hypoxic conditions in an LCN2-dependent manner: Knockdown of LCN2 expression with shRNA inhibited LeptoM growth and promoted apoptosis in hypoxia (fig. S9, F to P), and overexpression of LCN2 provided resistance to hypoxic stress (fig. S9, Q and R). From these experiments, we conclude that cancer cell LCN2 expression supports cancer cell growth within hypoxic CSF in LM.

Cancer cells use LCN2 to collect sparse extracellular iron in the CSF

In the absence of disease, CSF contains minimal extracellular iron. To investigate the levels of this micronutrient in LM, we assayed total iron levels by mass spectroscopy in the CSF of cancer patients. We found that total iron concentration and the proportion of iron bound to LCN2 was increased in the CSF of patients with LM relative to patients without LM (fig. S10, A and B). In addition, patient CSF LCN2 levels correlated with iron concentration (table S3). Reflecting the importance of inflammatory signaling, CSF iron levels also correlated with IL-6 and hepcidin.

Turning to our mouse models, we found that LCN2 gene expression was up-regulated in LeptoM cells relative to Par cells (figs. S4D and S10C). In vivo, LCN2 knockdown by shRNA was partially rescued through addition of iron-loaded transferrin (Fig. 5, A and B, and fig. S10, D to F), which suggests that iron transport plays a key role in LCN2-dependent cancer cell

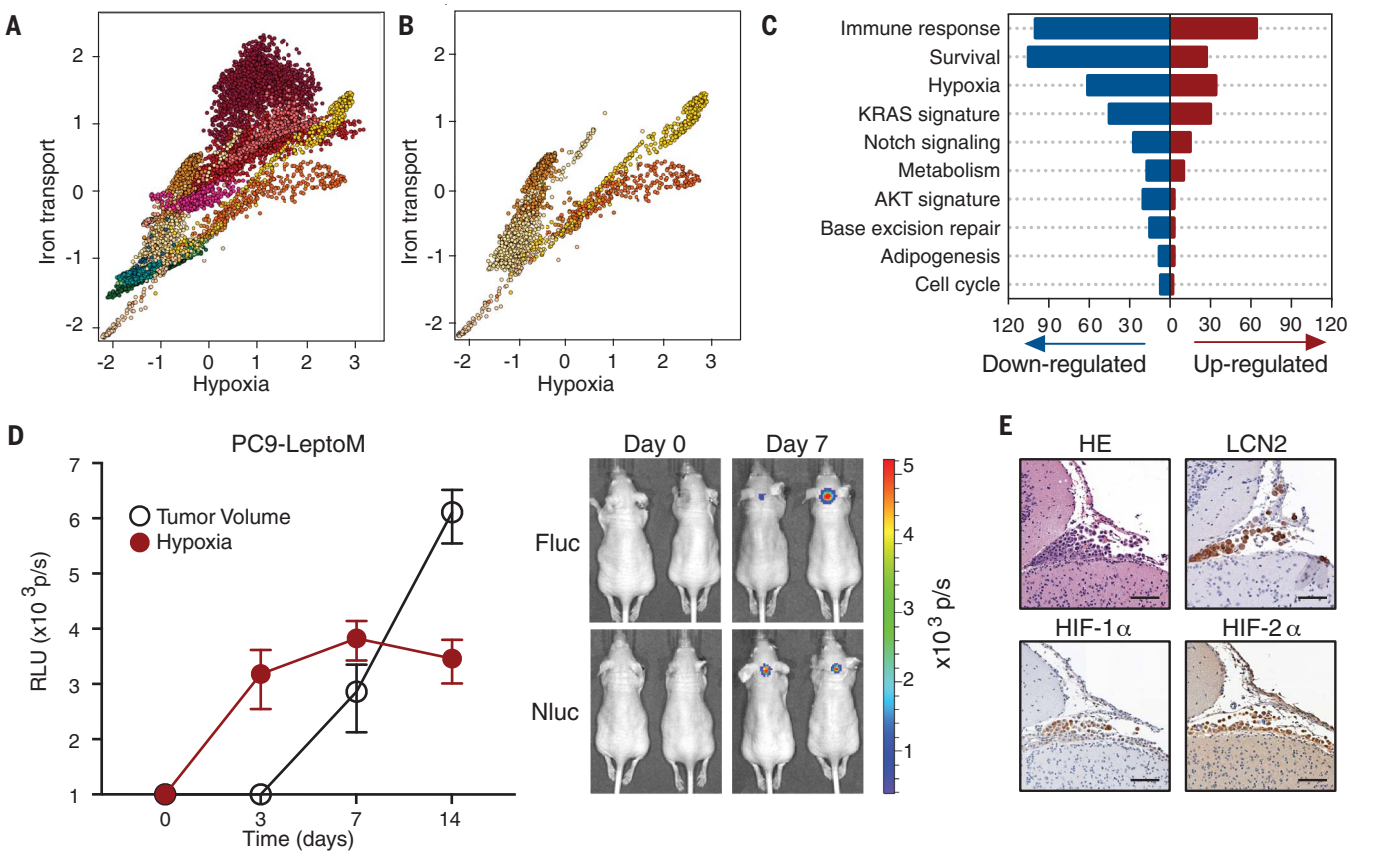

Fig. 4. LCN2 supports cancer cell growth in the hypoxic CSF microenvironment. (**A**) Correlation between hypoxia and iron ion transport gene signatures. Axis value represents mean gene signature expression per cell, standardized to have zero mean and unit of standard deviation. Each dot represents a cell, colored by cell type as in Fig. 1B. (**B**) Cancer cell populations from (A) alone. (**C**) Gene set enrichment (GSA) analysis of PC9 and LLC models by bulk RNA sequencing of LeptoM shCtl and shLCN2. Numbers of significantly up-regulated (red) and down-regulated (blue) genes in GSA analysis are indicated on the *x* axis; $n = 2$ per group. $P < 0.05$. See also fig. S7B. (**D**) Leptomeningeal tumor growth in a dual-reporter in vivo system. PC9-LeptoM cells express Firefly luciferase (Fluc) constitutively; NanoLuc (Nluc) is induced downstream of the hypoxia response element. Left: Fluc and Nluc are assayed by BLI at indicated time points. Solid circles indicate Nluc; open circles indicate Fluc. Right: Representative BLI images at day 0 and day 7. $n = 8$ to 10 per group in each of two independent experiments. Data are means ± SEM. (**E**) Leptomeningeal tissue sections stained with hematoxylin and eosin (HE) and immunohistochemistry for LCN2 and hypoxia-inducible factors HIF-1α and HIF-2α in PC9-LeptoM model. Scale bars, 50 μm.

growth in the CSF. To investigate this further, we examined iron uptake in these LeptoM cells in vitro. Inhibition of either SLC22A17 or LCN2 expression in LeptoM cells by shRNA in vitro inhibited iron accumulation and cell growth (fig. S10, G to I). Intracellular iron accumulation and cell growth were rescued by addition of exogenous transferrin (fig. S10, G to I).

Activated macrophages cannot generate reactive oxygen species unless iron concentrations are sufficiently high (*22*). We hypothesized that macrophages within the CSF, particularly in LM, have lower iron stores than macrophages circulating in the blood. To address this, we studied the syngeneic LLC-LeptoM mouse model (table S2). We collected macrophages from either the CSF or the spleen in the setting of LM or after challenge with LPS (Fig. 5F). We found that the intracellular iron content of CSF macrophages declined significantly in the setting of LM when compared with LPS treatment (Fig. 5C and fig. S10J). We also found that shRNA-mediated knockdown of cancer cell LCN2 expression increased macrophage iron content (Fig. 5C and fig. S10K). Finally, we found that the impairment of iron uptake in the CSF has functional consequences for these macrophages: Both respiratory burst and phagocytosis were impaired in the setting of LM in a LCN2-dependent fashion (Fig. 5, D and E). Together, these observations are consistent with a model in which inflammatory signals promote cancer cell LCN2 production. This in turn allows cancer cells to acquire the iron that is present in limiting amounts in CSF, which not only supports their own growth but inhibits iron uptake and iron-dependent functional activities of macrophages.

Analysis of iron chelation therapy for LM in mice

Because iron is limiting in the CSF, we reasoned that iron chelation might impair cancer cell growth in the CSF and tested this hypothesis in our mouse models (table S2). We inoculated recipient mice with either MDA231-LeptoM or PC9-LeptoM cells and treated them intracisternally with vehicle, the iron chelator deferoxamine (DFO), or the copper chelator D-penicillamine (D-Pen) on day 0 or day 7 after engraftment and every 3 days thereafter (fig. S11, A and B). DFO treatment substantially suppressed iron levels within the LeptoM cells as well as their growth (Fig. 5F and fig. S11, C to F). Notably, DFO treatment conferred a survival benefit to the MDA231 and PC9 mouse models relative to vehicle control (Fig. 5G, fig. S11, G and H, and table S4). As expected for this chelator treatment, we found that iron concentration in the CSF from DFO-treated mice was decreased at day 28 relative to that in control mice (fig. S11, I and J). The number of CSF macrophages was slightly reduced by the D-Pen or DFO treatment, whereas the numbers of neutrophils, T cells, and monocytes were not affected (fig. S11, K and L).

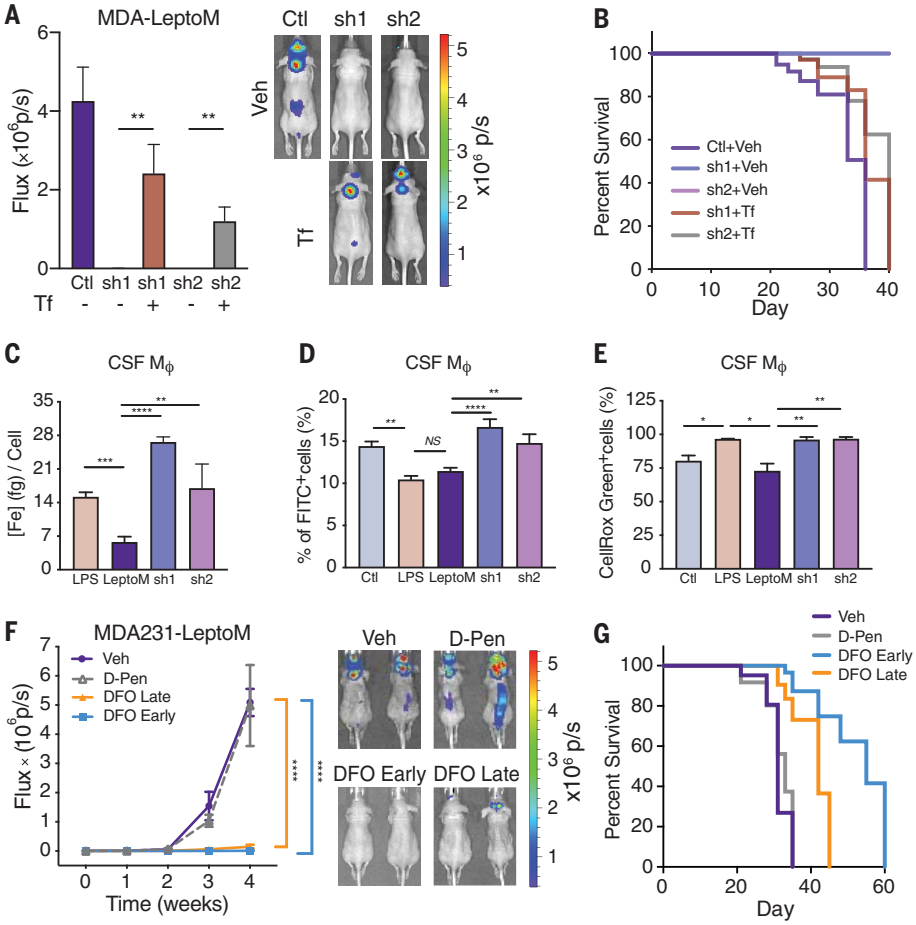

Fig. 5. LCN2 transports iron to support cancer cell growth. (**A**) Tumor growth in mice injected with MDA231-LeptoM cells expressing shCtl or shLCN2. Treatment with either vehicle or diferric holotransferrin (Tf; 5 mg/ml) began on day 1 and continued every third day for a total of seven doses. Left: Histogram represents in vivo BLI imaging after inoculation at day 21; n = 8 to 10 per group in each of two independent experiments. Right: Representative BLI images. $^{**}P < 0.01$ (unpaired t test). Data are means ± SEM. (**B**) Kaplan-Meier survival curve of LeptoM groups from (A). sh1 + Veh versus sh1 + Tf, $P < 0.0001$. sh2 + Veh versus sh2 + Tf, $P < 0.0001$. (**C**) Soluble iron concentration from macrophages collected from CSF in LPS-stimulated, LeptoM, or LeptoM-shLCN2 (sh1 and sh2) mouse model at day 14. Soluble iron was measured by mass spectroscopy. n = 4 per group. $^{**}P < 0.01$, $^{***}P < 0.001$, $^{****}P < 0.0001$ (unpaired t test). Data are means ± SEM. (**D** and **E**) Phagocytosis (D) and reactive oxygen species (ROS) generation (E) in CSF-derived macrophages by flow cytometric analysis after LeptoM (LLC model), shLCN2 LPS, or vehicle (Ctl) treatment. Phagocytosis was detected by fluorescein isothiocyanate (FITC)–labeled *Escherichia coli*; CellROX Green$^+$ cells represent percent of live cells with ROS. n = 12 to 15 (Ctl), n = 4 or 5 (LPS), n = 11 to 18 (LeptoM), n = 8 (shLCN2). $^*P < 0.05$, $^{**}P < 0.01$, $^{****}P < 0.0001$ (unpaired t test). Data are means ± SEM (two independent experiments). (**F**) Tumor growth in MDA231-LeptoM model after chelator treatment: deferoxamine (DFO) or D-penicillamine (D-Pen) on day 0 (early) or day 7 (late); see also fig. S11. Left: Results from in vivo BLI imaging on day 28 after inoculation; n = 8 to 10 per group in each of two independent experiments. Right: Representative BLI images. $^{****}P < 0.0001$. Data are means ± SEM. (**G**) Kaplan-Meier survival curve of mice treated in (F). $P < 0.0001$.

Discussion

Circulating immune cells routinely encounter nutritionally sparse environments as they migrate from the circulation into the tissues. Indeed, immune cells use a discrete set of transcriptional programs to make use of limited resources, including iron and oxygen. In the case of inflammatory macrophages, interferon-γ signaling promotes the generation of nitric oxide (*23*), impairing oxidative phosphorylation (*24*) and allowing for generation of reactive oxygen species (*25*).

Cancer cells cope with challenging environmental constraints differently from immune cells. The genetic heterogeneity of cancer cells provides these cells with a selective advantage over other cell types. To study cellular competition for sparse nutrients at human scale, we applied single-cell RNA-seq to patient-derived samples of LM, a lethal complication of cancer. In doing so, we uncovered a specific example of how the dynamic transcriptional heterogeneity of cancer cells can confer a functional selective advantage (*26*–*28*). We found that cancer cells make use of LCN2/SLC22A17, a high-affinity iron collection system that enables them to effectively outcompete other cells in the leptomeninges for sparse environmental iron. The other major iron-utilizing cell in the CSF, the macrophage, is rendered iron-deficient by this process, resulting in impaired respiratory burst and phagocytosis.

The leptomeninges pose unusual constraints on both the infiltrating immune system and cancer cells; we found that intercellular signaling is substantially altered within the leptomeningeal space. Investigators studying other experimental systems focused on extracranial sites have observed macrophage LCN2 generation (*29*), which promotes cancer cell migration and invasion (*13*, *30*). In LM, CSF macrophages do not produce LCN2. Rather, the inflammatory microenvironment promotes the generation of LCN2 in cancer cells. As obligate partners for cancer cell migration, invasion, and metastasis, tumor-associated macrophages are well known to alter the behavior of cancer cells (*31*). The evolutionary dynamics that we have discovered between malignant and nonmalignant cells within the leptomeninges reveal both the robust nature of cancer's transcriptional plasticity and microenvironmental vulnerabilities ripe for therapeutic exploitation.

REFERENCES AND NOTES

1. S. Kesari, T. T. Batchelor, *Neurol. Clin.* **21**, 25–66 (2003).
2. K. Oechsle, V. Lange-Brock, A. Kruell, C. Bokemeyer, M. de Wit, *J. Cancer Res. Clin. Oncol.* **136**, 1729–1735 (2010).
3. R. Spector, S. Robert Snodgrass, C. E. Johanson, *Exp. Neurol.* **273**, 57–68 (2015).
4. D. Subirá *et al.*, *Neuro-oncol.* **14**, 43–52 (2012).
5. E. Nemeth *et al.*, *J. Clin. Invest.* **113**, 1271–1276 (2004).
6. J. Yang *et al.*, *Mol. Cell* **10**, 1045–1056 (2002).
7. D. H. Goetz *et al.*, *Mol. Cell* **10**, 1033–1043 (2002).
8. L. Kjeldsen, D. F. Bainton, H. Sengeløv, N. Borregaard, *Blood* **83**, 799–807 (1994).
9. C. Mertens *et al.*, *PLOS ONE* **11**, e0166164 (2016).
10. C. Mertens *et al.*, *OncoImmunology* **7**, e1408751 (2017).
11. A. Boire *et al.*, *Cell* **168**, 1101–1113.e13 (2017).
12. M. Jung *et al.*, *Sci. Signal.* **9**, ra64 (2016).
13. L. R. Devireddy, C. Gazin, X. Zhu, M. R. Green, *Cell* **123**, 1293–1305 (2005).
14. I. Mosialou *et al.*, *Nature* **543**, 385–390 (2017).
15. N. Hamzic, A. Blomqvist, C. Nilsberth, *J. Neuroendocrinol.* **25**, 271–280 (2013).
16. Q. Liu, M. Nilsen-Hamilton, *J. Biol. Chem.* **270**, 22565–22570 (1995).
17. T. H. Flo *et al.*, *Nature* **432**, 917–921 (2004).
18. A. R. Moschen *et al.*, *Cell Host Microbe* **19**, 455–469 (2016).
19. D. M. Mosser, J. P. Edwards, *Nat. Rev. Immunol.* **8**, 958–969 (2008).
20. S. V. Torti, F. M. Torti, *Nat. Rev. Cancer* **13**, 342–355 (2013).
21. J. H. Cha *et al.*, *Nat. Commun.* **5**, 4952 (2014).
22. G. Cairo, S. Recalcati, A. Mantovani, M. Locati, *Trends Immunol.* **32**, 241–247 (2011).

23. R. J. Arts *et al.*, *Cell Metab.* **24**, 807–819 (2016).
24. J. Van den Bossche *et al.*, *Cell Rep.* **17**, 684–696 (2016).
25. E. L. Mills *et al.*, *Cell* **167**, 457–470.e13 (2016).
26. E. Azizi *et al.*, *Cell* **174**, 1293–1308.e36 (2018).
27. I. Tirosh *et al.*, *Science* **352**, 189–196 (2016).
28. Y. Lavin *et al.*, *Cell* **169**, 750–765.e17 (2017).
29. M. Jung *et al.*, *Mol. Cell. Biol.* **32**, 3938–3948 (2012).
30. X. Duan *et al.*, *Int. J. Physiol. Pathophysiol. Pharmacol.* **10**, 105–114 (2018).
31. J. Condeelis, J. W. Pollard, *Cell* **124**, 263–266 (2006).
32. A. Gayoso, J. Shor, Doublet Detection (version v2.4). Zenodo, DOI:10.5281/zenodo.2658730 (2018).
33. F. A. Wolf, P. Angerer, F. J. Theis, *Genome Biol.* **19**, 15 (2018).
34. L. Haghverdi, A. T. L. Lun, M. D. Morgan, J. C. Marioni, *Nat. Biotechnol.* **36**, 421–427 (2018).
35. J. H. Levine *et al.*, *Cell* **162**, 184–197 (2015).
36. L. McInnes, J. Healy, J. Melville, arXiv 1802.03426 [stat.ML] (6 December 2018).
37. D. van Dijk *et al.*, *Cell* **174**, 716–729.e27 (2018).
38. M. D. Turner, B. Nedjai, T. Hurst, D. J. Pennington, *Biochim. Biophys. Acta* **1843**, 2563–2582 (2014).
39. G. Finak *et al.*, *Genome Biol.* **16**, 278 (2015).
40. R. R. Coifman, M. Maggioni, S. W. Zucker, I. G. Kevrekidis, *Curr. Opin. Neurobiol.* **15**, 576–584 (2005).
41. M. Setty *et al.*, *Nat. Biotechnol.* **37**, 451–460 (2019).
42. A. Subramanian *et al.*, *Proc. Natl. Acad. Sci. U.S.A.* **102**, 15545–15550 (2005).
43. J. C. Reijneveld, M. J. Taphoorn, E. E. Voest, *J. Neurooncol.* **42**, 137–142 (1999).
44. Y. Ushio, N. L. Chernik, J. B. Posner, W. R. Shapiro, *J. Neuropathol. Exp. Neurol.* **36**, 228–244 (1977).
45. D. X. Nguyen *et al.*, *Cell* **138**, 51–62 (2009).
46. O. Butovsky *et al.*, *Nat. Neurosci.* **17**, 131–143 (2014).
47. M. I. Love, W. Huber, S. Anders, *Genome Biol.* **15**, 550 (2014).
48. V. K. Mootha *et al.*, *Nat. Genet.* **34**, 267–273 (2003).

ACKNOWLEDGMENTS

We are deeply grateful to the patients and families who donated clinical samples for this research. **Funding:** Supported by National Cancer Institute (NCI) grants P30 CA008748 and R35 CA220508 (C.I.-D.) and NCI grant 1U2CCA233284 (D.P.), Pew Charitable Trusts grant GC241069 (A.B.), Damon Runyon Cancer Research Foundation grant GC240764 (A.B.), Pershing Square Sohn Cancer Research Alliance grant GC239280 (A.B.), the Baker Family Foundation (A.B.), American Brain Tumor Association grant BRF1900019 (J.R. and A.B.), the Robert J. Kleberg Jr. and Helen C. Kleberg Foundation (C.I.-D.), and the Alan and Sandra Gerry Metastasis and Tumor Ecosystems Center (D.P.). **Author contributions:** A.B. and Y.C. conceived the project; A.B., Y.C., and J.R. designed the experiments; Y.C., J.R., and C.D. performed mouse work; V.K., L.M., and D.P. performed and analyzed scRNA-seq experiments; U.S. collected and clinically annotated human spinal fluid; T.B. and C.I.-D. collected and analyzed autopsy tissues and spinal fluid; C.D., M.A., F.S., and K.N. performed ELISAs and immunohistochemistry; T.T. performed all mass spectroscopy work; and Y.C., J.R., and A.B. wrote the manuscript. **Competing interests:** A.B. is an inventor on U.S. provisional patent application 62/258,044, "Modulating Permeability of the Blood Cerebrospinal Fluid Barrier," filed by Memorial Sloan Kettering Cancer Center. A.B. is an unpaid member of the Scientific Advisory Board of EVREN Technologies. **Data and materials availability:** Single-cell and bulk RNA-sequencing data have been deposited to NCBI GEO as GSE150681 SuperSeries. Cell lines LLC-LeptoM, PC9-LeptoM, and MDA231-LeptoM are available from A.B.

SUPPLEMENTARY MATERIALS

science.sciencemag.org/content/369/6501/276/suppl/DC1
Materials and Methods
Figs. S1 to S11
Tables S1 to S7
References (*32*–*48*)

View/request a protocol for this paper from *Bio-protocol*.

21 August 2019; accepted 1 June 2020
10.1126/science.aaz2193